https://doi.org/10.5194/acp-2020-1247
Preprint. Discussion started: 24 March 2021

Atmospheric Chemistry and Physics Discussions

Physical and chemical constraints on transformation and mass-increase of fine aerosols in northeast Asia

Saehee Lim[a], Meehye Lee[a,*], Paolo Laj[b,c], Sang-Woo Kim[d], Kang-Ho Ahn[e], Junsoo Gil[a], Xiaona Shang[a,f], Marco Zanatta[g], and Kyeong-Sik. Kang[h]

[a] Dept. of Earth and Environmental Sciences, Korea University, Seoul, 02841, South Korea

[b] Univ. Grenoble-Alpes, CNRS, IRD, Grenoble INP, Institute for Geosciences and Environmental Research (IGE), Grenoble, 38000, France

[c] Dept. of Physics, University of Helsinki, Helsinki, 00014, Finland

[d] School of Earth and Environmental Sciences, Seoul National University, Seoul, 08826, South Korea

[e] Dept. of Mechanical Engineering, Hanyang University, Ansan-si, Gyeonggi-do, 15588, South Korea

[f] Shanghai Key Laboratory of Atmospheric Particle Pollution and Prevention (LAP3), Department of Environmental Science & Engineering, Institute of Atmospheric Sciences, Fudan University, Shanghai, 200438, China

[g] Alfred Wegener Institute (AWI), Helmholtz Center for Polar and Marine Research, Bremerhaven, Germany

[h] Jeju Air Quality Research Center, National Institute of Environmental Research, Aewol, Jeju, 63040, South Korea

*Correspondence to: M. Lee (meehye@korea.ac.kr)

https://doi.org/10.5194/acp-2020-1247
Preprint. Discussion started: 24 March 2021

Atmospheric Chemistry and Physics Discussions

Abstract

Over the past few decades, northeast Asia has suffered from the extreme levels of $PM_{2.5}$ (particulate matter with an aerodynamic diameter smaller than 2.5 μm). Despite extensive efforts and the scientific advances in understanding $PM_{2.5}$ pollution, the fundamental mechanisms responsible for the occurrence of high $PM_{2.5}$ concentrations have not been comprehensively understood. In this study, we investigated the physical and chemical drivers for the formation and transformation of atmospheric particles using a four-year dataset of nanoparticle number size distributions, $PM_{2.5}$ chemical composition, gaseous precursors, and meteorological variables in northeast Asia outflows. The empirical orthogonal function (EOF) analyses of size-separated particle numbers extracted two modes representing a burst of nanoparticles (EOF1) and an increase in $PM_{2.5}$ mass (EOF2) associated with persistent anticyclone and synoptic-scale stagnation, respectively. The vertical structure of the particles demonstrated that the synoptic conditions also affected the daily evolution of boundary layer, promoting either the formation of nanoparticles through deep mixing or conversion into accumulation-mode particles in shallow mixed layers. In the haze-development episode equivalent to EOF2 during the KORUS-AQ (KORea-US Air Quality) campaign, the $PM_{2.5}$ mass reached 63 μg m^{-3} with the highest contribution from inorganic constituents, which was accompanied by a thick coating of refractory black carbon (rBC) that linearly increased with condensation-mode particles. This observational evidence suggests that the thick coating of rBC resulted from an active conversion of condensable gases into particle-phase on the BC surface, thereby increasing the mass of the accumulation-mode aerosol. Consequently, this result complies with the strategy to reduce black carbon as a way to effectively mitigate haze pollution as well as climate change in northeast Asia.

Keywords: aerosol number concentration, new particle formation, $PM_{2.5}$, haze, boundary layer, black carbon

ABBREVIATIONS

EOF: empirical orthogonal function; SIA: secondary inorganic aerosols; NPF: new particle formation; CS: condensation sink; SOR: sulfur oxidation ratio; NOR: nitrogen oxidation ratio; GR: growth rate; OC: organic carbon; EC: elemental carbon; CBH: cloud base height; MLH: mixed layer height; DRH: deliquescence relative humidity; PBL: planetary boundary layer; rBC: refractory black carbon; KORUS-AQ: Korea–US Air Quality

https://doi.org/10.5194/acp-2020-1247
Preprint. Discussion started: 24 March 2021

Atmospheric Chemistry and Physics Discussions

1. Introduction

Countries in northeast Asia have experienced severe atmospheric pollution over the past few decades. Severe and persistent haze pollution with high levels of $PM_{2.5}$ (particulate matter with aerodynamic diameter smaller than 2.5 μm) has been the primary public issue, particularly in terms of its strong relationship with adverse human health impacts, such as cardiovascular and respiratory disease and lung cancer, both of which lead to increased risk of mortality (Apte et al., 2018; Atkinson et al., 2015; Burnett et al., 2018; Lelieveld et al., 2015). In Seoul, the capital of South Korea, the annual $PM_{2.5}$ concentration has remained consistently as high as 20-30 μg m^{-3} during the past decade (Yeo et al., 2019), easily exceeding the national annual air quality standard (15 μg m^{-3}) as well as the World Health Organization (WHO) annual air quality standard (10 μg m^{-3}). High-concentration $PM_{2.5}$ events tend to occur frequently in the cold months from November to March (Lim et al., 2012, 2014), when daily mean $PM_{2.5}$ concentrations often exceed the Korean daily air quality standard (35 μg m^{-3}) with a composition dominated by secondary inorganic aerosols (SIA), namely SO_4^{-2}, NO_3^-, and NH_4^+. In contrast to the role of SIA as an important driver of high $PM_{2.5}$ levels in cold months, organic carbonaceous aerosol accounts for a large proportion in fine aerosol mass during warm months (e.g., Kim et al., 2018). Meanwhile, black carbon (BC), a strong climate-forcing agent (Bond et al., 2013; Boucher et al., 2013), has been recently known that its insoluble and inert nature facilitate its long-range transport across China during haze pollution events (Wang et al., 2016; Zheng et al., 2019). The characteristic occurrence of $PM_{2.5}$ events has been commonly observed over the northeast Asia region (Fan et al., 2020; Liu et al., 2018).

Long-term regulatory actions to control emissions have been implemented in South Korea as well as China. However, severe haze events have been unpredictable and more frequent over the last couple of years in Seoul (Park et al., 2021). Existing knowledge does not explicitly explain the complex processes responsible for the occurrence of high $PM_{2.5}$ concentration (e.g., An et al., 2019). Most of all, the relevant chemical (trans)formation mechanisms and meteorological contributions as well as emission sources that are vital for the effective mitigation of haze pollution, have yet to be fully identified.

Theoretically, the formation of aerosol particles begins with new particle formation (NPF) and subsequent growth; aerosols are formed via the gas-to-particle conversion of condensable gases, which include SO_2, NOx, VOCs, and NH_3. This process, known as NPF, is dependent primarily upon two parameters: (i) a source strength of condensable gas and (ii) a level of pre-existing particles that act as a condensation sink (CS). In a polluted urban environment, such as China and India, NPF often occurs under high levels of both condensable gases and CS, both resulting in a high growth rate of particles, unlike the clean European environment (Chu et al., 2019; Mönkkönen et al., 2005; Wu et al., 2007). In a sulfur-rich environment, such as northeast Asia (China and Korea) (Yao et al., 2018), NPF is highly sensitive to meteorological conditions that control the levels of both condensable gas and CS (Song et al., 2010; Quan et al., 2017; Wang et al., 2014). However, the processes

https://doi.org/10.5194/acp-2020-1247
Preprint. Discussion started: 24 March 2021

Atmospheric Chemistry and Physics Discussions

responsible for particle growth and the further increase in fine-aerosol mass may not be explained in the same manner across the Asian continent. In China, NPF events often occurred during haze-pollution episodes or led to high concentrations of $PM_{2.5}$ (Guo et al., 2014; Wiedensohler et al., 2009). Nanoparticles formed through NPF continued to grow to condensation mode (~100 to 200 nm) or further to droplet mode (~400 to 500 nm) particles, which can contribute to fine aerosol mass (e.g., Guo et al., 2014). In contrast, such a phenomenon has rarely been observed in Seoul or at background sites in South Korea (e.g., Kim et al., 2013). Therefore, the conditions and mechanisms responsible for the rapid increase in $PM_{2.5}$ mass are still poorly understood.

In this regard, we analyzed the size-separated number distributions of nanoparticles in conjunction with the $PM_{2.5}$ chemical composition, gaseous precursors, and meteorological variables in the East Asia outflow region. Based on the results, we aimed to elucidate the mechanisms of transformation of number-dominated or mass-dominated particles and to constrain key physical and chemical drivers.

2. Methods

2.1 Measurements

We measured aerosol number concentrations, the mass concentrations of $PM_{2.5}$ and its chemical constituents, the mixing ratios of reactive gases, and meteorological parameters at the Jeju Air quality Monitoring Research Center (33.21° N, 126.23° E, 600 m asl; hereinafter referred to “Aewol”) in Jeju island, South Korea (Fig. S1), from January 2013 to December 2016. This station has been served as the national background air pollution monitoring station without evidently significant local pollution sources.

The number concentrations of size-separated particles at aerosol diameter (Dp) ranging from 10.4 to 469.8 nm were measured every 30 min using a Scanning Mobility Particle Sizer (SMPS, TSI, USA). $PM_{2.5}$ mass concentrations were continuously measured using a beta attenuation mass monitor (Thermo Scientific, USA). For $PM_{2.5}$ chemical composition, water-soluble ions and carbon components (organic carbon, OC; and elemental carbon, EC) were determined. Water-soluble ions of $PM_{2.5}$ were measured with a Monitor for Aerosols. & Gases in Ambient Air (MARGA, Metrohm, Swiss) every hour. In addition, OC and EC concentrations were simultaneously analyzed using a Sunset Lab OCEC Analyzer (Sunset Laboratory Inc., USA). Reactive gases including CO, NO_2, NH_3, and O_3 were continuously monitored. Meteorological parameters including temperature, relative humidity, wind speed, wind direction, and cloud base height were obtained from Korean Meteorological administration (KMA, https://data.kma.go.kr/cmmn/main.do). All measurements were assimilated into one-hour averages. In addition, SO_2 was further measured at Gosan Climate Observatory (GCO, 33.17° N, 126.10° E) in Jeju island. To find collective evidence, another set of the cloud base height measurement by ceilometer at GCO, were incorporated into the results of Aewol.

https://doi.org/10.5194/acp-2020-1247
Preprint. Discussion started: 24 March 2021

Atmospheric Chemistry and Physics Discussions

In addition, the Korea–US Air Quality (KORUS-AQ) campaign provided a unique opportunity to observe distinctive events from May to June 2016, during which the vertical profiles of size-segregated aerosol number concentrations and meteorological parameters were obtained by balloon measurements in SMA (in specific, Ansan (33.17° N, 126.10° E, 70 m asl) and Icheon (37.27° N, 127.43° E), which are satellite cities of Seoul; Fig. S1). The balloon measurements were conducted in Ansan at 11:26-11:45 a.m. in local time on 20 May and at 8:55-09:05 a.m. and 16:05-16:13 p.m. on 25 May. The aerosol number concentrations in size ranges of Dp>3.5 nm, 0.3 μm<Dp<0.5 μm, and 0.5 μm <Dp<1.0 μm were measured by a Condensation Particle Counter (CPC) and two Optical Particle Counters (OPC), respectively (Querol et al., 2017, 2018). Together with the physical properties of refractory BC (Sect. 2.2), the vertical profiles were used in the subsequent analyses of this study.

To add data interpretation, aerosol liquid water (ALW) content was calculated in "forward mode" using the ISORROPIA-II thermodynamic model (Fountoukis and Nenes, 2007).

2.1 Single Particle Soot Photometer

In parallel, during the KORUS-AQ campaign at GCO, the physical properties of refractory BC (number and mass concentrations, size distributions, and coating thickness of rBC) were determined using the Single Particle Soot Photometer (Droplet Measurement Technology, Boulder, CO, USA) (Moteki and Kondo, 2010; Schwarz et al., 2006; Stephens et al., 2003).

The SP2 uses a laser-induced incandescence technique to quantify the mass of a single refractory BC (Petzold et al., 2013), was utilized to determine the mass concentration, size distribution, and mixing state of rBC particles. The incandescence signal was calibrated using well-characterized fullerene soot particles (Alfa Aesar; #FS12S011), and the scattering detector was calibrated with a spherical polystyrene latex size standard (Thermo Scientific, formerly Duke Scientific) (Baumgardner et al., 2012; Laborde et al., 2012b). The detection range of a single-particle mass is 0.33–128 fg, corresponding to rBC mass equivalent diameters (D_{rBC} = 70–514 nm), assuming a void-free material density of 1.8 g cm^{-3} (Bond et al., 2006). To correct for the rBC mass outside the lower detection limit, the rBC mass size distribution was fitted with a lognormal function, and a correction was achieved by adding 10% of the total uncorrected rBC mass on average. An rBC mass larger than the upper detection limit was treated as the largest mass detectable. Basically, using the leading-edge-only approach (Gao et al., 2007; Laborde et al., 2012a), the optical diameter of the rBC-containing particle, D_{shell}, was inferred from the leading-edge scattering signal using Mie theory with refractive indices of $1.5 - 0i$ and $2.26 - 1.26i$ for the rBC coating material and rBC core, respectively, at an SP2 operating wavelength of 1064 nm. The coating thickness of the rBC particle was determined as $(D_{shell} - D_{rBC})/2$ and was restricted to the rBC core with a D_{rBC} of 200 ± 20 nm. Coating was defined as a coating thickness ≥10 nm, considering the systematic uncertainty in

https://doi.org/10.5194/acp-2020-1247
Preprint. Discussion started: 24 March 2021

Atmospheric Chemistry and Physics Discussions

estimating the coating thickness (Laborde et al., 2012a). For the concentration, size distribution, and mixing state of rBC particles, data were averaged hourly to be comparable to hourly-based $PM_{2.5}$ chemical properties.

3. Results and Discussion

3.1. The characteristic variation of $PM_{2.5}$ concentration

The $PM_{2.5}$ concentration of Aewol was much lower as a background site than that of Seoul (Fig. 1). In Seoul, the annual mean $PM_{2.5}$ concentration ranged from 27.3 μg m^{-3} to 38.3 μg m^{-3} during 2013 ~ 2016, exceeding the national annual air quality standard (15 μg m^{-3}) every year. For the same period, the annual $PM_{2.5}$ concentration was 13.9 ~ 19.7 μg m^{-3} at Aewol. The daily mean $PM_{2.5}$ concentration violated the standard (35 μg m^{-3}) by 33% and 9% of the entire period in Seoul and Aewol, respectively. Despite the difference in $PM_{2.5}$ level, the seasonal variation was similar at the two sites with high levels in the cold months, demonstrating the enhancement of wintertime $PM_{2.5}$ is a significant regional issue over the east Asia (Fan et al., 2020; Li et al., 2020; Liu et al., 2018).

3.2. Detecting the two modes of particle number distributions

Continuous measurements of size-separated number concentrations, spanning four years from 2013 to 2016, were analyzed using an empirical orthogonal function (EOF) method (e.g., Kim et al., 2014). Consequently, two largest modes explained 64% of the total variation; the first mode explains a considerable portion (55%) of the total variability, the second mode accounted for 9% of the total variation, and each of the other modes accounted for less than 4%. The first and second modes clearly showed contrast in terms of the diurnal evolution of the particle number concentrations and dominant particle sizes (Fig. 2). The difference between the two modes is explicitly demonstrated in the average number-size distribution of the particles for the top 10 % days with the highest principle component (PC) scores (Fig. S2a). Thereinafter, these cases were considered to be representative of the two modes and referred to as “EOF1” and “EOF2”, respectively. Out of the four-year measurement period, each 143 days were categorized as EOF1 and EOF2, respectively. While EOF1 frequently occurred in May and October, the monthly frequency of EOF2 was high in March and June (Fig. S2b and c). In EOF2, the mode of number, surface area, and volume was larger in size, compared to EOF 1(Fig. S3). Using these particle number distributions, CS was calculated for the entire range of diameters from 10 nm to 470 nm (Text S1) (Kulmala and Kerminen, 2008). In addition, EOF1 and EOF2 were compared each other for $PM_{2.5}$, including SO_4^{2-}, NO_3^-, and NH_4^+ (namely, SIA), and the reactive gases in terms of the sulfur oxidation ratio

https://doi.org/10.5194/acp-2020-1247
Preprint. Discussion started: 24 March 2021

Atmospheric Chemistry and Physics Discussions

(SOR), nitrogen oxidation ratio (NOR), and ammonia conversion ratio (Fig. 3).

In EOF1, the variation of the number concentration is equivalent to what used to be observed during the NPF and growth event, with the maximum number concentration greater than 10^4 cm^{-3} at ~20–30 nm around noon (Fig. 2c). The nucleation-mode particles dominated number concentrations with a mean $GR_{10\text{-}30}$ of 2.28 ± 1.99 nm h^{-1} (growth rate of particles at 10–30 nm in diameter; Table 1 and Text S1), which was close to the lower bound of the growth rate (GR) observed across China (1–15 nm h^{-1}; Chu et al., 2019 and references therein) and in the range of the global GR (1–10 nm h^{-1}; Nieminen et al., 2018 and references therein). In this case, the levels of condensable gases, such as SO_2 and NOx, were higher by 45% and 14%, respectively, relative to the mean of the entire period (Fig. 3a). In contrast, $CS_{100\text{-}470nm}$ equal to 1.26 ± 0.86 (Table 1 and Text S1) was relatively lower than the mean (Fig. 3a). Thus, EOF1, characterized by the dominant nucleation-mode particles and relatively high condensable gases and low CS, clearly represent the NPF.

In comparison, for EOF2, the accumulation-mode particles are dominantly distributed throughout the day (Fig. 2d). As the number concentration of accumulation-mode particles increased in the afternoon through the evening, the maximum concentration reached 5000 cm^{-3} at 100–130 nm; in addition, the mode of the volume concentration was found to be at larger sizes over 300 nm (Fig. S3). In this case, the level of condensable gases was noticeably lower, with higher $CS_{100\text{-}470nm}$ (1.76 ± 1.04) than that of EOF1 (Table 1). The large surface areas of pre-existing particles would strongly suppress NPF, as newly formed clusters are scavenged by pre-existing particles before reaching observable sizes of 3-nm diameters (Kulmala et al., 2017; Kulmala and Kerminen, 2008). It turned out that on the days of EOF2 that was the second principal component of the EOF analysis, the characteristics of the particles and precursors are completely opposite to those of EOF1 days. It is noteworthy that EOF2 as well as EOF1 occurred the most frequently in March, when $PM_{2.5}$ concentration is the highest in Korea including Jeju and Seoul (Fig. 1 & Fig.S2). If EOF1 actually represents the NPF event responsible for the increase in aerosol number, then the physical and chemical properties of EOF2 can be regarded as conditions for the increase in aerosol mass.

3.3. Meteorological constraints and chemical consequences

The chemical properties of the two modes were clearly distinguished by the level of precursor gases and $PM_{2.5}$ chemical compositions, which were evidently coupled with meteorological conditions.

NPF is known to be sensitive to meteorological conditions. In accordance with what has been reported in previous studies, EOF1 mode was frequently observed on sunny and clear days in the study region, where it was situated under a high-pressure system after frontal passage (Chu et al., 2019; Dall'Osto et al., 2018) during

https://doi.org/10.5194/acp-2020-1247
Preprint. Discussion started: 24 March 2021


Atmospheric Chemistry and Physics Discussions

spring and fall (Fig. 4a and Fig. S2b). This mode occurred under lower ambient temperature and relative humidity and under higher solar radiation with less cloud coverage, compared with EOF2 (Table 1). The predominant northerly winds (Fig. 4a and Fig. S4) brought dry air with relatively high levels of SO_2 (Liang et al., 2016; Tian et al., 2019; Wu et al., 2007), and the concentrations of all precursor gases were increased in the afternoon (Fig. 3a). The meteorological conditions and the SO_2 level and its diurnal variation imply the efficient conversion of SO_2 to H_2SO_4, leading to NPF (Spracklen et al., 2006). In contrast to the precursor gases, SO_4^{2-} concentration was half that of EOF2 and even lower than the mean of the entire experiment (Table 1 and Fig. 3).

The mean $PM_{2.5}$ concentration of EOF2 was 26.5 ± 21.3 μg m^{-3}, being higher by 40% than EOF1 (19.1± 15.0 μg m^{-3}). The chemical composition of $PM_{2.5}$ was dominated by SIA, with a mean contribution of 41% to the mass (20% SO_4^{2-}, 10% NO_3^-, 10% NH_4^+) (Table 1). Of the days exceeding the daily Korean air quality threshold value during the four-year period, 10% and 29% belong to EOF1 and EOF2, respectively. Particularly, EOF2 days with $PM_{2.5}$ concentrations above the national standard were mostly observed in cold months, for which the $PM_{2.5}$ concentration and contribution of SIA was noticeably elevated. Therefore, it is reasonable to argue that EOF2 represents a unique condition favorable for an increase in $PM_{2.5}$ mass concentration, which is particularly driven by SIA. The mean geopotential height reveals that the EOF2 was associated with synoptic-scale stagnation (Fig. 4b). As shown in Fig. 4b, slow, and thus humid by picking up water vapor over the sea, westerly winds were dominant throughout the EOF2 periods (Fig. 4b and Table 1). The diurnal variation in SIA concentrations (Fig. 3) closely follows the hourly contribution of westerly winds (Fig. S4c). Although photochemical activity is expected to be weak owing to a low solar radiation intensity with a high amount of cloud coverage for EOF2, SOR was significantly elevated and $PM_{2.5}$ chemical constituents were completely neutralized (equivalent ratio of $([SO_4^{2-}] + [NO_3^-])/[NH_4^+] = 1$) (Table 1). In contrast, the mean mass fraction of EC and its diurnal variation remained almost the same between the two modes.

Clearly, the typical meteorological conditions differ between the two modes and so do their chemical properties, leading to different consequences in aerosol number size distributions. In this context, questions arise as to what physical and chemical mechanisms cause such differences in the two modes. Based on the findings above, we particularly focus on the EOF2 period in the subsequent analyses.

3.4. Chemical evolution coupled with boundary layer expansion

Recently, boundary layer processes were found to play a crucial role in increasing $PM_{2.5}$ concentration through vertical diffusion and aerosol dispersion (Ding et al., 2016; Miao et al., 2017; Ye et al., 2016). In addition, entrainment through the boundary layer has been suggested as an important mechanism for enhancing surface O_3 (Hu et al., 2018; Lee et al., 2003). For NPF, the combined effect of boundary layer dynamics and atmospheric

https://doi.org/10.5194/acp-2020-1247
Preprint. Discussion started: 24 March 2021

Atmospheric Chemistry and Physics Discussions

chemistry on aerosol composition was emphasized (Hao et al., 2018; Song et al., 2010). In this study, the concentrations of all precursor gases were elevated in the afternoon for both cases, when the boundary layer was expanded the most (Fig. 3).

Therefore, the evolution of the boundary layer was investigated based on the cloud base height (CBH), which was continuously monitored. A mid-low CBH corresponds fairly well to a maximum mixed layer height (MLH) particularly in the afternoon (Huang et al., 2018; Seidel et al., 2010). Meanwhile, the hourly averaged CBH exhibits a clear diurnal variation, similar to the typical MLH (Fig. 3). Moreover, in addition to the chemical properties of gases and aerosols, the cloud coverage and CBH were distinguished between the two periods; for EOF2, a higher cloud coverage, a lower CBH, and consequently lower solar radiation intensity, relative to the another period.

In EOF1, under a high-pressure system, the radiation heating under the high pressure caused the boundary layer to be unstable, leading to strong vertical mixing and a weak inversion. Meanwhile, the greater cloud coverage with the lower CBH resulted in a stable boundary layer and strong inversion in EOF2 under stagnant conditions (Table 1 and Fig. 3). The deep vertical mixing diluted the pre-existing particles, resulting in CS lowered. All gaseous precursors, including SO_2, increased in concentration at surface, whereas SOR was slightly decreased in the afternoon (Fig. 3a). The gas-phase oxidation of SO_2 by OH is a slow process, with a corresponding SO_2 lifetime of 5–10 days. In contrast, NOR slightly increased in the afternoon, suggesting the photochemical production of nitrate (Fig. 3a) through gaseous oxidation and subsequent gas–solid equilibrium under low temperature and relative humidity below the deliquescence relative humidity (DRH) for NH_4NO_3 during the day.

In comparison, for EOF2, particle number concentration was low at night and in the morning; however, it gradually increased during the day, reaching its maximum in the late afternoon (Fig. 2d). In urban areas with heavy local emissions, a strong inversion forces the local circulation to be confined to the atmospheric boundary layer under undesirable ventilation, thereby acting as a lid; thus, pollutants are accumulated within the boundary layer (e.g., Ning et al., 2018; Ye et al., 2016). In contrast to the heavily polluted sites, in the background or outflow sites, the significant elevation in aerosol concentration during the day is believed to occur primarily by the intrusion of pollutants carried from the upper atmospheric layer, e.g., residual layer formed at night or free troposphere, upon the expansion of the planetary boundary layer (PBL). Evidently, the $PM_{2.5}$ mass increased during the daytime when the PBL was expanded and the wind direction was shifted to a westerly flow (Fig. 3b and S4). Therefore, the rapid increase in $PM_{2.5}$ mass accompanying the development of the PBL was conspicuously explained by the entrainment of particles transported from upstream areas.

To further examine the role of the boundary layer, specific cases corresponding to EOF1 and EOF2 were explored. The vertical profiles of particle number concentrations and meteorological variables were obtained

https://doi.org/10.5194/acp-2020-1247
Preprint. Discussion started: 24 March 2021

Atmospheric Chemistry and Physics Discussions

from balloon measurements in satellite cities of Seoul during the two periods (18-22 May and 25-27 May) of the KORUS-AQ campaign. It provides a unique opportunity to investigate the relationship between the boundary layer and aerosol chemical evolution. The profiles from May 20 and May 25 contrast the atmospheric conditions of "persistent anticyclone" and "low-level transport and haze development", leading to an enhanced ozone production and a high $PM_{2.5}$ concentration, respectively (Peterson et al., 2019). Likewise, the aerosol number size distributions were obviously different in Jeju during these two periods that are categorized as EOF1 and EOF2, respectively, based on the EOF analysis in previous sections (Fig. 5). Hereafter, the two important periods during the campaign referred to as "EOF1 case" and "EOF2 case", respectively, which were compared for meteorology and atmospheric chemical properties in subsequent sections (Table 2).

The high surface temperature resulted in a deep mixing layer on May 20 ("EOF1 case") (Fig. 6a). The particle number concentrations at all size ranges decreased with the altitude, revealing the dilution of pre-existing particles by vertical mixing.

In contrast, in the morning on May 25 ("EOF2 case"), the mixed layer was shallow with a temperature inversion layer at about 1000 m (top gray box in Fig. 6b). The morning profile illustrates visibly high concentrations of the particle$_{>3.5\ nm}$ (about 10^4 cm^{-3}) both at surface and at around the inversion (gray boxes in Fig. 6b). The latter was similar to the previous observation of a considerably large number of ultrafine particles commonly found above the cloud (Clarke, 1993). While the former was attributed to an effect of fresh emissions in the morning, even higher concentration of the particle$_{>3.5\ nm}$ at around the inversion can be reasonably explained by another process. In the afternoon, the large amount of particle$_{>3.5\ nm}$ observed in the morning (Fig. 6b) collapsed at around 1000 m, but below which the layer was well-mixed in terms of particle concentrations (Fig. 6c). The evolution of particle vertical profile demonstrates the possible processes as follows; an entrainment of nanoparticles transported from upstream areas and carried through the upper layer, trapping of the particles in residual layer at night, and their traveling down toward boundary layer after subsequential break-up of the inversion and a mixing of air within the mixed layer during day.

Furthermore, in the mixed layer, the concentrations of particle$_{0.3\text{-}0.5\ \mu m}$ and particle$_{0.5\text{-}1.0\ \mu m}$ remarkably increased relative to those in the morning (gray box in Fig. 6c). This feature was more clearly observed in the upper layer than surface, indicating an effect of condensational and/or hygroscopic growth of particles rather than an effect of emissions from surface. The vertical profiles indicate that the particle number concentrations were significantly affected by ambient RH. Compared to the EOF1 case with a deep vertical mixing and dilution, the EOF2 case was characterized by discernable layers in the vertical structure of meteorological variables including RH, temperature, and wind direction. Such a shallow mixed layer of low temperature and high RH is favorable for condensation of precursors and hygroscopic growth of particles, thereby greatly affecting the

https://doi.org/10.5194/acp-2020-1247
Preprint. Discussion started: 24 March 2021

Atmospheric Chemistry and Physics Discussions

concentration and size distribution of particles.

We considered the deliquescence relative humidity (DRH) of inorganic salts, such as NH_4NO_3 and $(NH_4)_2SO_4$, as a crucial factor for the rapid particle growth, because the SIA was the predominant constituent of $PM_{2.5}$ during the KORUS-AQ period (Jordan et al., 2020). In the morning, the burst of particle$_{>3.5\ nm}$ above 10^4 was found near the surface and just above the inversion layer with RH below the DRHs of both $(NH_4)_2SO_4$ and NH_4NO_3 (Fig. 6b). This layered structure became uniform in the afternoon with the development of the boundary layer, resulting in the noticeable reduction in the number of particle$_{>3.5\ nm}$ at altitudes between 1000 m and 1500 m (Fig. 6c). Here, RH increased well above the DRH of NH_4NO_3 and the number concentration of particle$_{0.3\text{-}0.5\ \mu m}$ and particle$_{0.5\text{-}1.0\ \mu m}$ was noticeably increased. In contrast, the number of particle$_{>3.5\ nm}$ tended to be backed up below 1000 m. The mixing through the inversion layer can cause gas-to-particle partitioning and further hygroscopic growth, leading to an increase in the number of accumulation-mode particles. Considering the fact that the synoptic circulation is the main factor determining the level of atmospheric constituents over the Korean peninsula (Jordan et al., 2020; Peterson et al., 2019), this process would have been active throughout the entire EOF2 period.

Therefore, the vertical profiles of nanoparticles and their evolution during the EOF2 case suggest that the entrainment of nanoparticles from the upper layer into the shallow and humid boundary layer and the increase in their size via hygroscopic growth, consequently contributing to increase in $PM_{2.5}$ mass concentration. In fact, the $PM_{2.5}$ mass concentration increased at Aewol, up to 63 μg m^{-3} (Table 2), as well as Seoul during the EOF2 case (Jordan et al., 2020). Recently, it was suggested that pollutants were carried from the upstream areas in the upper layer by westerly winds, remained above the nocturnal boundary layer, and entrained into the PBL during the day; this led to a high PM_{10} concentration at the surface (Lee et al., 2019). Similarly, the evolution of the boundary layer played a key role in the increase in $PM_{2.5}$ mass under EOF2 conditions.

3.5. rBC as a robust tracer for particle growth in size and mass

In addition to the evolution of the boundary layer, the role of accumulation-mode particles in increasing the aerosol surface and mass was highlighted above. Among aerosol particles, BC is of particular interest, as bare BC particle is insoluble and small, generally peaking below 100 nm in diameter and thus it potentially provides a chemically inert surface on which volatile substances can condense to form a coating and further grow on. In terms of climate effect, BC has been well established as the second strongest warming agent after CO_2 (Bond et al., 2013). To assess a role of BC particle in aerosol transformation, the mass and mixing state of rBC particles were determined at GCO and compared between the two periods of the KORUS-AQ campaign (EOF1 case and EOF2 case) (Table 2 and Fig. 6).

https://doi.org/10.5194/acp-2020-1247
Preprint. Discussion started: 24 March 2021


Atmospheric Chemistry and Physics Discussions

When the $PM_{2.5}$ mass concentration was highly elevated over the Korean peninsula during EOF2 case (May 25–27) (Jordan et al., 2020), the coating of rBC was noticeably thick (48 ± 39 nm) relative to other period of the campaign (Fig. 7a). Together with the enhanced SIA concentrations and the thicker coating of rBC, the aerosol liquid water content (ALWC) was as high as 10.3±8.2 μg m^{-3} (Fig. 7b and Table 2). Given that the RH remained high at greater than 60% during the day and up to 90% at night (Fig. 7b), gas-to-particle conversion and hygroscopic growth of NH_4NO_3 and $(NH_4)_2SO_4$ by uptake of water were expected to be promoted, leading to a large increase in ALWC. SOR was almost linearly increased with RH (Fig. S5b and d). More importantly, it is known that sulfuric acid readily condenses on the rBC surface (Kiselev et al., 2010; Zhang et al., 1993, 2008), which provides an active surface for heterogeneous reaction by changing its hygroscopic properties (Khalizov et al., 2009). Hence, the characteristic features observed during the transport and haze period suggest an effective condensation of precursors to SIA and its growth on the rBC surface, forming thick coating on it, during the transport of air masses (Adachi et al., 2014; Lim et al., 2018; Ueda et al., 2016). As coated with inorganic salts, the shell size of rBC with a core diameter of 200 nm reached approximately 300 nm. Given that the $PM_{2.5}$ concentration increased linearly with the volume concentration of $particles_{200\text{-}470\ nm}$ (Fig. 7a), the role of internally-mixed BC particles is critical to the increase in the mass of accumulation-mode aerosol, as they provide surfaces for precursors of SIA to condense on.

In contrast, a thinner coating (29 ± 31 nm) and a lower concentration (by 40%) of rBC particles as well as the low levels of SIA were evident under low RH (53 ± 9%) conditions during EOF1 case (May 18–20). In this case, the organic carbon (OC) fraction was the greatest in $PM_{2.5}$. ALWC was very low as well. It is likely that the weather condition suppressed the condensation of volatile materials on aerosol surface and thus the secondary aerosol formation on rBC surface. It is also possible that organic materials may form an organic film on the BC surface, inhibiting the uptake of SIA and increase of the rBC coating (Saxena et al., 1995; Sellegri et al., 2003). Instead, they promoted the growth of nucleation-mode particles smaller than 60 nm under low RH conditions (Fig. 7a). The mass size distributions of OC, NO_3^-, and SO_4^{-2} estimated by the aerosol mass spectrometer generally show organics enriched in nucleation-mode particles (e.g., Kang et al., 2018; Kim et al., 2018).

In this regard, the coating thickness of rBC particle is suggested to be a useful parameter to understand the chemical mechanisms responsible for the occurrence of SIA-driven fine aerosol pollution. This, in turn, implies that reducing BC emissions will be one of the effective ways to combat high $PM_{2.5}$ mass concentrations in northeast Asia, especially during the cold months.

4. Conclusions

https://doi.org/10.5194/acp-2020-1247
Preprint. Discussion started: 24 March 2021

Atmospheric Chemistry and Physics Discussions

In Jeju, a background site, in the northeast Asia, the four-year (2013-2016) dataset of nanoparticle distributions, $PM_{2.5}$ chemical composition, and gaseous precursors were analyzed together with the vertical profiles of nanoparticles and rBC properties that were measured during the KORea-US Air Quality (KORUS-AQ) study. An empirical orthogonal function (EOF) analysis of the size-separated number distribution distinguished the two types of diurnal evolution of nanoparticles. Their occurrence was intimately coupled with synoptic atmospheric conditions, which creates preconditions for the burst in nucleation-mode (EOF1) and the mass increase in accumulation-mode (EOF2) particles. These two orthogonal modes were consistently applicable to the distinct episodes ("persistent anticyclone" and "low-level transport and haze development") observed during the KORUS-AQ campaign. A high-pressure system promotes instability of the boundary layer and deep vertical mixing, resulting in new particle formation (NPF) and growth event. In contrast, under synoptic-scale stagnation, secondary inorganic aerosol (SIA), such as $(NH_4)_2SO_4(s)$ or $NH_4NO_3(s)$, likely formed above the boundary layer while the air was slowly transported, entrained into the shallow boundary layer upon vertical mixing, and condensed onto the pre-existing particles at high RH exceeding the DRH of those inorganic salts, leading to an increase in $PM_{2.5}$ mass. Not to mention, RH played a critical role in this process, and the estimated aerosol liquid water content reached 30~40 % of the average $PM_{2.5}$ mass. In addition, the first measurement sets of rBC properties at Jeju demonstrates the convincing evidence that BC particles provide surfaces for SIA to condense and form coating on, facilitating an increase in aerosol mass, particularly in the accumulation-mode. In the haze development period equivalent to EOF2, $PM_{2.5}$ mass increased with major inorganic composition, and the coating thickness and mass of BC was increased proportionally with the condensation mode-particles.

As a result, the coating thickness of rBC is hypothesized to serve as a proxy indicating the occurrence of SIA-driven high $PM_{2.5}$ mass in the study region. Consequently, our result supports strategies for reducing emissions of BC particles that provides the co-benefits of mitigating fine aerosol pollution and climate change.

Acknowledgement

This research was supported by the National Strategic Project-Fine Particle of the National Research Foundation of Korea (NRF), funded by the Ministry of Science and ICT (MSIT), Ministry of Environment (ME), and Ministry of Health and Welfare (MOHW) (2017M3D8A1092015). M. Lee thanks to the support by the National Research Foundation of Korea (NRF) (2020R1A2C301459211). Funding to S. Lim was provided by the National Research Foundation of Korea (NRF) from the Ministry of Science and ICT (2016R1D1A1B03934532 and 2018R1D1A1B07050849). S.-W. Kim was supported by the Basic Science Research Program through the

https://doi.org/10.5194/acp-2020-1247
Preprint. Discussion started: 24 March 2021

National Research Foundation of Korea (NRF), funded by the Ministry of Education (2017R1D1A1B06032548). Funding to K.-S. Kang was provided by the National Institute of Environmental Research (NIER-RP2017-166).

References

Adachi, K., Zaizen, Y., Kajino, M. and Igarashi, Y.: Mixing state of regionally transported soot particles and the coating effect on their size and shape at a mountain site in Japan, J. Geophys. Res. Atmos., 119(9), 5386–5396, doi:10.1002/2013JD020880, 2014.

An, Z., Huang, R.-J., Zhang, R., Tie, X., Li, G., Cao, J., Zhou, W., Shi, Z., Han, Y., Gu, Z. and Ji, Y.: Severe haze in northern China: A synergy of anthropogenic emissions and atmospheric processes., Proc. Natl. Acad. Sci. U. S. A., 116(18), 8657–8666, doi:10.1073/pnas.1900125116, 2019.

Apte, J. S., Brauer, M., Cohen, A. J., Ezzati, M. and Pope, C. A.: Ambient $PM_{2.5}$ Reduces Global and Regional Life Expectancy, Environ. Sci. Technol. Lett., 5(9), 546–551, doi:10.1021/acs.estlett.8b00360, 2018.

Atkinson, R. W., Mills, I. C., Walton, H. A. and Anderson, H. R.: Fine particle components and health—a systematic review and meta-analysis of epidemiological time series studies of daily mortality and hospital admissions, J. Expo. Sci. Environ. Epidemiol., 25(2), 208–214, doi:10.1038/jes.2014.63, 2015.

Baumgardner, D., Popovicheva, O., Allan, J., Bernardoni, V., Cao, J., Cavalli, F., Cozic, J., Courcoux, Y., Diapouli, E., Eleftheriadis, K., Genberg, P. J., Gonzalez, C., Gysel, M., John, A., Kirchstetter, T. W., Kuhlbusch, T. a. J., Laborde, M., Lack, D., Müller, T., Niessner, R., Petzold, A., Piazzalunga, A., Putaud, J. P., Schwarz, J., Sheridan, P., Subramanian, R., Swietlicki, E., Valli, G., Vecchi, R. and Viana, M.: Soot reference materials for instrument calibration and intercomparisons: a workshop summary with recommendations, Atmos. Meas. Tech., 5(2), 1869–1887, doi:10.5194/amtd-5-2315-2012, 2012.

Bond, T. C., Habib, G. and Bergstrom, R. W.: Limitations in the enhancement of visible light absorption due to mixing state, J. Geophys. Res., 111(D20), D20211, doi:10.1029/2006JD007315, 2006.

Bond, T. C., Doherty, S. J., Fahey, D. W., Forster, P. M., Berntsen, T., DeAngelo, B. J., Flanner, M. G., Ghan, S., Kärcher, B., Koch, D., Kinne, S., Kondo, Y., Quinn, P. K., Sarofim, M. C., Schultz, M. G., Schulz, M., Venkataraman, C., Zhang, H., Zhang, S., Bellouin, N., Guttikunda, S. K., Hopke, P. K., Jacobson, M. Z., Kaiser, J. W., Klimont, Z., Lohmann, U., Schwarz, J. P., Shindell, D., Storelvmo, T., Warren, S. G. and Zender, C. S.: Bounding the role of black carbon in the climate system: A scientific assessment, J. Geophys. Res. Atmos., 118(11), 5380–5552, doi:10.1002/jgrd.50171, 2013.

https://doi.org/10.5194/acp-2020-1247
Preprint. Discussion started: 24 March 2021

Atmospheric Chemistry and Physics Discussions

Boucher, O., Randall, D., Artaxo, P., Bretherton, C., Feingold, G., Forster, P., Kerminen, V.-M., Kondo, Y., Liao, H., Lohmann, U., Rasch, P., Satheesh, S. K., Sherwood, S., Stevens, B. and Zhang, X. Y.: Clouds and Aerosols, in Climate Change 2013: The Physical Science Basis. Contribution of Working Group I to the Fifth Assessment Report of the Intergovernmental Panel on Climate Change, edited by V. B. and P. M. M. Stocker, T.F., D. Qin, G.-K. Plattner, M. Tignor, S.K. Allen, J. Boschung, A. Nauels, Y. Xia, pp. 571–657, Cambridge University Press, United Kingdom and New York, NY, USA., 2013.

Burnett, R., Chen, H., Szyszkowicz, M., Fann, N., Hubbell, B., Pope, C. A., Apte, J. S., Brauer, M., Cohen, A., Weichenthal, S., Coggins, J., Di, Q., Brunekreef, B., Frostad, J., Lim, S. S., Kan, H., Walker, K. D., Thurston, G. D., Hayes, R. B., Lim, C. C., Turner, M. C., Jerrett, M., Krewski, D., Gapstur, S. M., Diver, W. R., Ostro, B., Goldberg, D., Crouse, D. L., Martin, R. V, Peters, P., Pinault, L., Tjepkema, M., van Donkelaar, A., Villeneuve, P. J., Miller, A. B., Yin, P., Zhou, M., Wang, L., Janssen, N. A. H., Marra, M., Atkinson, R. W., Tsang, H., Quoc Thach, T., Cannon, J. B., Allen, R. T., Hart, J. E., Laden, F., Cesaroni, G., Forastiere, F., Weinmayr, G., Jaensch, A., Nagel, G., Concin, H. and Spadaro, J. V: Global estimates of mortality associated with long-term exposure to outdoor fine particulate matter., Proc. Natl. Acad. Sci. U. S. A., 115(38), 9592–9597, doi:10.1073/pnas.1803222115, 2018.

Chu, B., Kerminen, V.-M., Bianchi, F., Yan, C., Petäjä, T. and Kulmala, M.: Atmospheric new particle formation in China, Atmos. Chem. Phys., 19(1), 115–138, doi:10.5194/acp-19-115-2019, 2019.

Clarke, A. D.: Atmospheric nuclei in the Pacific midtroposphere: Their nature, concentration, and evolution, J. Geophys. Res., 98(D11), 20633, doi:10.1029/93JD00797, 1993.

Dall'Osto, M., Beddows, D. C. S., Asmi, A., Poulain, L., Hao, L., Freney, E., Allan, J. D., Canagaratna, M., Crippa, M., Bianchi, F., de Leeuw, G., Eriksson, A., Swietlicki, E., Hansson, H. C., Henzing, J. S., Granier, C., Zemankova, K., Laj, P., Onasch, T., Prevot, A., Putaud, J. P., Sellegri, K., Vidal, M., Virtanen, A., Simo, R., Worsnop, D., O'Dowd, C., Kulmala, M. and Harrison, R. M.: Novel insights on new particle formation derived from a pan-european observing system, Sci. Rep., 8(1), 1482, doi:10.1038/s41598-017-17343-9, 2018.

Ding, A. J., Huang, X., Nie, W., Sun, J. N., Kerminen, V. -M., Petäjä, T., Su, H., Cheng, Y. F., Yang, X. -Q., Wang, M. H., Chi, X. G., Wang, J. P., Virkkula, A., Guo, W. D., Yuan, J., Wang, S. Y., Zhang, R. J., Wu, Y. F., Song, Y., Zhu, T., Zilitinkevich, S., Kulmala, M. and Fu, C. B.: Enhanced haze pollution by black carbon in megacities in China, Geophys. Res. Lett., 43(6), 2873–2879, doi:10.1002/2016GL067745, 2016.

Fan, H., Zhao, C. and Yang, Y.: A comprehensive analysis of the spatio-temporal variation of urban air pollution in China during 2014–2018, Atmos. Environ., 220, 117066, doi:10.1016/J.ATMOSENV.2019.117066, 2020.

https://doi.org/10.5194/acp-2020-1247
Preprint. Discussion started: 24 March 2021

Atmospheric Chemistry and Physics Discussions

460 Fountoukis, C. and Nenes, A.: ISORROPIA II: a computationally efficient thermodynamic equilibrium model
461 for K+- Ca2+-Mg2+-NH+ 4 -Na+-SO2− 4 -NO− 3 -Cl−-H2O aerosols, Atmos. Chem. Phys., 7(17), 4639–
462 4659, doi:10.5194/acp-7-4639-2007, 2007.

463 Gao, R. S., Schwarz, J. P., Kelly, K. K., Fahey, D. W., Watts, L. A., Thompson, T. L., Spackman, J. R.,
464 Slowik, J. G., Cross, E. S., Han, J.-H., Davidovits, P., Onasch, T. B. and Worsnop, D. R.: A novel method for
465 estimating light-scattering properties of soot aerosols using a modified single-particle soot photometer,
466 Aerosol Sci. Technol., 41(2), 125–135, doi:10.1080/02786820601118398, 2007.

467 Guo, S., Hu, M., Zamora, M. L., Peng, J., Shang, D., Zheng, J., Du, Z., Wu, Z., Shao, M., Zeng, L., Molina,
468 M. J. and Zhang, R.: Elucidating severe urban haze formation in China., Proc. Natl. Acad. Sci. U. S. A.,
469 111(49), 17373–8, doi:10.1073/pnas.1419604111, 2014.

470 Hao, L., Garmash, O., Ehn, M., Miettinen, P., Massoli, P., Mikkonen, S., Jokinen, T., Roldin, P., Aalto, P.,
471 Yli-Juuti, T., Joutsensaari, J., Petäjä, T., Kulmala, M., Lehtinen, K. E. J., Worsnop, D. R. and Virtanen, A.:
472 Combined effects of boundary layer dynamics and atmospheric chemistry on aerosol composition during new
473 particle formation periods, Atmos. Chem. Phys., 18(23), 17705–17716, doi:10.5194/acp-18-17705-2018,
474 2018.

475 Hu, J., Li, Y., Zhao, T., Liu, J., Hu, X.-M., Liu, D., Jiang, Y., Xu, J. and Chang, L.: An important mechanism
476 of regional O3 transport for summer smog over the Yangtze River Delta in eastern China, Atmos. Chem.
477 Phys., 18(22), 16239–16251, doi:10.5194/acp-18-16239-2018, 2018.

478 Huang, Q., Cai, X., Wang, J., Song, Y. and Zhu, T.: Climatological study of the boundary-layer air stagnation
479 index for China and its relationship with air pollution, Atmos. Chem. Phys., 18(10), 7573–7593,
480 doi:10.5194/acp-18-7573-2018, 2018.

481 Jordan, C., Crawford, J. H., Beyersdorf, A. J., Eck, T. F., Halliday, H. S., Nault, B. A., Chang, L.-S., Park, J.,
482 Park, R., Lee, G., Kim, H., Ahn, J., Cho, S., Shin, H. J., Lee, J. H., Jung, J., Kim, D.-S., Lee, M., Lee, T.,
483 Whitehill, A., Szykman, J., Schueneman, M. K., Campuzano-Jost, P., Jimenez, J. L., DiGangi, J. P., Diskin,
484 G. S., Anderson, B. E., Moore, R. H., Ziemba, L. D., Fenn, M. A., Hair, J. W., Kuehn, R. E., Holz, R. E.,
485 Chen, G., Travis, K., Shook, M., Peterson, D. A., Lamb, K. D. and Schwarz, J. P.: Investigation of factors
486 controlling $PM_{2.5}$ variability across the South Korean Peninsula during KORUS-AQ, Elem Sci Anth, 8(1), 28,
487 doi:10.1525/elementa.424, 2020.

488 Kang, E., Lee, M., Brune, W. H., Lee, T., Park, T., Ahn, J. and Shang, X.: Photochemical aging of aerosol
489 particles in different air masses arriving at Baengnyeong Island, Korea, Atmos. Chem. Phys., 18(9), 6661–
490 6677, doi:10.5194/acp-18-6661-2018, 2018.

https://doi.org/10.5194/acp-2020-1247
Preprint. Discussion started: 24 March 2021

Atmospheric Chemistry and Physics Discussions

491 Khalizov, A. F., Xue, H., Wang, L., Zheng, J. and Zhang, R.: Enhanced light absorption and scattering by
492 carbon soot aerosol internally mixed with sulfuric acid., J. Phys. Chem. A, 113(6), 1066–74,
493 doi:10.1021/jp807531n, 2009.

494 Kim, H., Zhang, Q. and Heo, J.: Influence of intense secondary aerosol formation and long-range transport on
495 aerosol chemistry and properties in the Seoul Metropolitan Area during spring time: results from KORUS-
496 AQ, Atmos. Chem. Phys., 18(10), 7149–7168, doi:10.5194/acp-18-7149-2018, 2018.

497 Kim, Y., Yoon, S.-C., Kim, S.-W., Kim, K.-Y., Lim, H.-C. and Ryu, J.: Observation of new particle formation
498 and growth events in Asian continental outflow, Atmos. Environ., 64, 160–168,
499 doi:10.1016/J.ATMOSENV.2012.09.057, 2013.

500 Kim, Y., Kim, S.-W. and Yoon, S.-C.: Observation of new particle formation and growth under cloudy
501 conditions at Gosan Climate Observatory, Korea, Meteorol. Atmos. Phys., 126(1–2), 81–90,
502 doi:10.1007/s00703-014-0336-2, 2014.

503 Kiselev, A., Wennrich, C., Stratmann, F., Wex, H., Henning, S., Mentel, T. F., Kiendler-Scharr, A., Schneider,
504 J., Walter, S. and Lieberwirth, I.: Morphological characterization of soot aerosol particles during LACIS
505 Experiment in November (LExNo), J. Geophys. Res., 115(D11), D11204, doi:10.1029/2009JD012635, 2010.

506 Kulmala, M. and Kerminen, V.-M.: On the formation and growth of atmospheric nanoparticles, Atmos. Res.,
507 90(2–4), 132–150, doi:10.1016/J.ATMOSRES.2008.01.005, 2008.

508 Kulmala, M., Kerminen, V.-M., Petäjä, T., Ding, A. J. and Wang, L.: Atmospheric gas-to-particle conversion:
509 why NPF events are observed in megacities?, Faraday Discuss., 200(0), 271–288, doi:10.1039/C6FD00257A,
510 2017.

511 Laborde, M., Mertes, P., Zieger, P., Dommen, J., Baltensperger, U. and Gysel, M.: Sensitivity of the Single
512 Particle Soot Photometer to different black carbon types, Atmos. Meas. Tech., 5(5), 1031–1043,
513 doi:10.5194/amt-5-1031-2012, 2012a.

514 Laborde, M., Schnaiter, M., Linke, C., Saathoff, H., Naumann, K.-H., Möhler, O., Berlenz, S., Wagner, U.,
515 Taylor, J. W., Liu, D., Flynn, M., Allan, J. D., Coe, H., Heimerl, K., Dahlkötter, F., Weinzierl, B., Wollny, A.
516 G., Zanatta, M., Cozic, J., Laj, P., Hitzenberger, R., Schwarz, J. P. and Gysel, M.: Single Particle Soot
517 Photometer intercomparison at the AIDA chamber, Atmos. Meas. Tech., 5, 3077–3097, doi:10.5194/amt-5-
518 3077-2012, 2012b.

519 Laborde, M., Crippa, M., Tritscher, T., Jurányi, Z., Decarlo, P. F., Temime-Roussel, B., Marchand, N.,

520 Eckhardt, S., Stohl, A., Baltensperger, U., Prévôt, A. S. H., Weingartner, E. and Gysel, M.: Black carbon
521 physical properties and mixing state in the European megacity Paris, Atmos. Chem. Phys., 13(11), 5831–
522 5856, doi:10.5194/acp-13-5831-2013, 2013.

523 Lee, H.-J., Jo, H.-Y., Kim, S.-W., Park, M.-S. and Kim, C.-H.: Impacts of atmospheric vertical structures on
524 transboundary aerosol transport from China to South Korea, Sci. Rep., 9(1), 13040, doi:10.1038/s41598-019-
525 49691-z, 2019.

526 Lee, S.-M., Fernando, H. J. S., Princevac, M., Zajic, D., Sinesi, M., McCulley, J. L. and Anderson, J.:
527 Transport and Diffusion of Ozone in the Nocturnal and Morning Planetary Boundary Layer of the Phoenix
528 Valley, Environ. Fluid Mech., 3(4), 331–362, doi:10.1023/A:1023680216173, 2003.

529 Lelieveld, J., Evans, J. S., Fnais, M., Giannadaki, D. and Pozzer, A.: The contribution of outdoor air pollution
530 sources to premature mortality on a global scale, Nature, 525(7569), 367–371, doi:10.1038/nature15371,
531 2015.

532 Li, M., Wang, L., Liu, J., Gao, W., Song, T., Sun, Y., Li, L., Li, X., Wang, Y., Liu, L., Daellenbach, K. R.,
533 Paasonen, P. J., Kerminen, V.-M., Kulmala, M. and Wang, Y.: Exploring the regional pollution characteristics
534 and meteorological formation mechanism of PM2.5 in North China during 2013–2017, Environ. Int., 134,
535 105283, doi:10.1016/J.ENVINT.2019.105283, 2020.

536 Liang, X., Li, S., Zhang, S., Huang, H. and Chen, S. X.: PM $_{2.5}$ data reliability, consistency, and air quality
537 assessment in five Chinese cities, J. Geophys. Res. Atmos., 121(17), 10,220-10,236,
538 doi:10.1002/2016JD024877, 2016.

539 Lim, S., Lee, M., Lee, G., Kim, S., Yoon, S. and Kang, K.: Ionic and carbonaceous compositions of PM10,
540 PM2.5 and PM1.0 at Gosan ABC Superstation and their ratios as source signature, Atmos. Chem. Phys.,
541 12(4), 2007–2024, doi:https://doi.org/10.5194/acp-12-2007-2012, 2012.

542 Lim, S., Lee, M., Kim, S.-W., Yoon, S.-C., Lee, G. and Lee, Y. J.: Absorption and scattering properties of
543 organic carbon versus sulfate dominant aerosols at Gosan climate observatory in Northeast Asia, Atmos.
544 Chem. Phys., 14(15), 7781–7793, doi:10.5194/acp-14-7781-2014, 2014.

545 Lim, S., Lee, M., Kim, S.-W. and Laj, P.: Sulfate alters aerosol absorption properties in East Asian outflow,
546 Sci. Rep., 8(1), 5172, doi:10.1038/s41598-018-23021-1, 2018.

547 Liu, Z., Gao, W., Yu, Y., Hu, B., Xin, J., Sun, Y., Wang, L., Wang, G., Bi, X., Zhang, G., Xu, H., Cong, Z.,
548 He, J., Xu, J. and Wang, Y.: Characteristics of PM2.5 mass concentrations and chemical species in urban and

https://doi.org/10.5194/acp-2020-1247
Preprint. Discussion started: 24 March 2021


Atmospheric Chemistry and Physics Discussions

549 background areas of China: emerging results from the CARE-China network, Atmos. Chem. Phys., 18(12),
550 8849–8871, doi:10.5194/acp-18-8849-2018, 2018.

551 Miao, Y., Guo, J., Liu, S., Liu, H., Li, Z., Zhang, W. and Zhai, P.: Classification of summertime synoptic
552 patterns in Beijing and their associations with boundary layer structure affecting aerosol pollution, Atmos.
553 Chem. Phys., 17(4), 3097–3110, doi:10.5194/acp-17-3097-2017, 2017.

554 Mönkkönen, P., Koponen, I. K., Lehtinen, K. E. J., Hämeri, K., Uma, R. and Kulmala, M.: Measurements in a
555 highly polluted Asian mega city: observations of aerosol number size distribution, modal parameters and
556 nucleation events, Atmos. Chem. Phys., 5(1), 57–66, doi:10.5194/acp-5-57-2005, 2005.

557 Moteki, N. and Kondo, Y.: Dependence of Laser-Induced Incandescence on Physical Properties of Black
558 Carbon Aerosols: Measurements and Theoretical Interpretation, Aerosol Sci. Technol., 44(8), 663–675,
559 doi:10.1080/02786826.2010.484450, 2010.

560 Nieminen, T., Kerminen, V.-M., Petäjä, T., Aalto, P. P., Arshinov, M., Asmi, E., Baltensperger, U., Beddows,
561 D. C. S., Beukes, J. P., Collins, D., Ding, A., Harrison, R. M., Henzing, B., Hooda, R., Hu, M., Hõrrak, U.,
562 Kivekäs, N., Komsaare, K., Krejci, R., Kristensson, A., Laakso, L., Laaksonen, A., Leaitch, W. R.,
563 Lihavainen, H., Mihalopoulos, N., Németh, Z., Nie, W., O'Dowd, C., Salma, I., Sellegri, K., Svenningsson,
564 B., Swietlicki, E., Tunved, P., Ulevicius, V., Vakkari, V., Vana, M., Wiedensohler, A., Wu, Z., Virtanen, A.
565 and Kulmala, M.: Global analysis of continental boundary layer new particle formation based on long-term
566 measurements, Atmos. Chem. Phys., 18(19), 14737–14756, doi:10.5194/acp-18-14737-2018, 2018.

567 Ning, G., Wang, S., Yim, S. H. L., Li, J., Hu, Y., Shang, Z., Wang, J. and Wang, J.: Impact of low-pressure
568 systems on winter heavy air pollution in the northwest Sichuan Basin, China, Atmos. Chem. Phys., 18(18),
569 13601–13615, doi:10.5194/acp-18-13601-2018, 2018.

570 Park, D.-H., Kim, S.-W., Kim, M.-H., Yeo, H., Park, S. S., Nishizawa, T., Shimizu, A. and Kim, C.-H.:
571 Impacts of local versus long-range transported aerosols on PM10 concentrations in Seoul, Korea: An estimate
572 based on 11-year PM10 and lidar observations, Sci. Total Environ., 750, 141739,
573 doi:10.1016/J.SCITOTENV.2020.141739, 2021.

574 Peterson, D. A., Hyer, E. J., Han, S.-O., Crawford, J. H., Park, R. J., Holz, R., Kuehn, R. E., Eloranta, E.,
575 Knote, C., Jordan, C. E. and Lefer, B. L.: Meteorology influencing springtime air quality, pollution transport,
576 and visibility in Korea, Elem Sci Anth, 7(1), 57, doi:10.1525/elementa.395, 2019.

577 Petzold, A., Ogren, J. A., Fiebig, M., Laj, P., Li, S.-M., Baltensperger, U., Holzer-Popp, T., Kinne, S.,
578 Pappalardo, G., Sugimoto, N., Wehrli, C., Wiedensohler, A. and Zhang, X.-Y.: Recommendations for

https://doi.org/10.5194/acp-2020-1247
Preprint. Discussion started: 24 March 2021

reporting “black carbon” measurements, Atmos. Chem. Phys., 13(16), 8365–8379, doi:10.5194/acp-13-8365-2013, 2013.

Quan, J., Liu, Y., Liu, Q., Jia, X., Li, X., Gao, Y., Ding, D., Li, J. and Wang, Z.: Anthropogenic pollution elevates the peak height of new particle formation from planetary boundary layer to lower free troposphere, Geophys. Res. Lett., 44(14), 7537–7543, doi:10.1002/2017GL074553, 2017.

Querol, X., Gangoiti, G., Mantilla, E., Alastuey, A., Minguillón, M. C., Amato, F., Reche, C., Viana, M., Moreno, T., Karanasiou, A., Rivas, I., Pérez, N., Ripoll, A., Brines, M., Ealo, M., Pandolfi, M., Lee, H.-K., Eun, H.-R., Park, Y.-H., Escudero, M., Beddows, D., Harrison, R. M., Bertrand, A., Marchand, N., Lyasota, A., Codina, B., Olid, M., Udina, M., Jiménez-Esteve, B., Soler, M. R., Alonso, L., Millán, M. and Ahn, K.-H.: Phenomenology of high-ozone episodes in NE Spain, Atmos. Chem. Phys., 17(4), 2817–2838, doi:10.5194/acp-17-2817-2017, 2017.

Querol, X., Alastuey, A., Gangoiti, G., Perez, N., Lee, H. K., Eun, H. R., Park, Y., Mantilla, E., Escudero, M., Titos, G., Alonso, L., Temime-Roussel, B., Marchand, N., Moreta, J. R., Revuelta, M. A., Salvador, P., Artíñano, B., García dos Santos, S., Anguas, M., Notario, A., Saiz-Lopez, A., Harrison, R. M., Millán, M. and Ahn, K.-H.: Phenomenology of summer ozone episodes over the Madrid Metropolitan Area, central Spain, Atmos. Chem. Phys., 18(9), 6511–6533, doi:10.5194/acp-18-6511-2018, 2018.

Saxena, P., Hildemann, L. M., McMurry, P. H. and Seinfeld, J. H.: Organics alter hygroscopic behavior of atmospheric particles, J. Geophys. Res., 100(D9), 18755, doi:10.1029/95JD01835, 1995.

Schwarz, J. P., Gao, R. S., Fahey, D. W., Thomson, D. S., Watts, L. a., Wilson, J. C., Reeves, J. M., Darbeheshti, M., Baumgardner, D. G., Kok, G. L., Chung, S. H., Schulz, M., Hendricks, J., Lauer, a., Kärcher, B., Slowik, J. G., Rosenlof, K. H., Thompson, T. L., Langford, a. O., Loewenstein, M. and Aikin, K. C.: Single-particle measurements of midlatitude black carbon and light-scattering aerosols from the boundary layer to the lower stratosphere, J. Geophys. Res., 111(D16), D16207, doi:10.1029/2006JD007076, 2006.

Seidel, D. J., Ao, C. O. and Li, K.: Estimating climatological planetary boundary layer heights from radiosonde observations: Comparison of methods and uncertainty analysis, J. Geophys. Res., 115(D16), D16113, doi:10.1029/2009JD013680, 2010.

Sellegri, K., Laj, P., Marinoni, A., Dupuy, R., Legrand, M. and Preunkert, S.: Contribution of gaseous and particulate species to droplet solute composition at the Puy de Dôme, France, Atmos. Chem. Phys., 3(5), 1509–1522, doi:10.5194/acp-3-1509-2003, 2003.

https://doi.org/10.5194/acp-2020-1247
Preprint. Discussion started: 24 March 2021

Song, M., Lee, M., Kim, J. H., Yum, S. S., Lee, G. and Kim, K.-R.: New particle formation and growth in relation to vertical mixing and chemical species during ABC-EAREX2005, Atmos. Res., 97(3), 359–370, doi:10.1016/J.ATMOSRES.2010.04.013, 2010.

Spracklen, D. V., Carslaw, K. S., Kulmala, M., Kerminen, V.-M., Mann, G. W. and Sihto, S.-L.: The contribution of boundary layer nucleation events to total particle concentrations on regional and global scales, Atmos. Chem. Phys., 6(12), 5631–5648, doi:10.5194/acp-6-5631-2006, 2006.

Stephens, M., Turner, N. and Sandberg, J.: Particle identification by laser-induced incandescence in a solid-state laser cavity., Appl. Opt., 42(19), 3726–3736, 2003.

Tian, P., Liu, D., Huang, M., Liu, Q., Zhao, D., Ran, L., Deng, Z., Wu, Y., Fu, S., Bi, K., Gao, Q., He, H., Xue, H. and Ding, D.: The evolution of an aerosol event observed from aircraft in Beijing: An insight into regional pollution transport, Atmos. Environ., 206, 11–20, doi:10.1016/J.ATMOSENV.2019.02.005, 2019.

Ueda, S., Nakayama, T., Taketani, F., Adachi, K., Matsuki, A., Iwamoto, Y., Sadanaga, Y. and Matsumi, Y.: Light absorption and morphological properties of soot-containing aerosols observed at an East Asian outflow site, Noto Peninsula, Japan, Atmos. Chem. Phys., 16(4), 2525–2541, doi:10.5194/acp-16-2525-2016, 2016.

Wang, D., Guo, H., Cheung, K. and Gan, F.: Observation of nucleation mode particle burst and new particle formation events at an urban site in Hong Kong, Atmos. Environ., 99, 196–205, doi:10.1016/J.ATMOSENV.2014.09.074, 2014.

Wang, Q., Huang, R.-J., Cao, J., Tie, X., Shen, Z., Zhao, S., Han, Y., Li, G., Li, Z., Ni, H., Zhou, Y., Wang, M., Chen, Y. and Su, X.: Contribution of regional transport to the black carbon aerosol during winter haze period in Beijing, Atmos. Environ., 132, 11–18, doi:10.1016/J.ATMOSENV.2016.02.031, 2016.

Wiedensohler, A., Cheng, Y. F., Nowak, A., Wehner, B., Achtert, P., Berghof, M., Birmili, W., Wu, Z. J., Hu, M., Zhu, T., Takegawa, N., Kita, K., Kondo, Y., Lou, S. R., Hofzumahaus, A., Holland, F., Wahner, A., Gunthe, S. S., Rose, D., Su, H. and Pöschl, U.: Rapid aerosol particle growth and increase of cloud condensation nucleus activity by secondary aerosol formation and condensation: A case study for regional air pollution in northeastern China, J. Geophys. Res., 114(D2), D00G08, doi:10.1029/2008JD010884, 2009.

Wu, Z., Hu, M., Liu, S., Wehner, B., Bauer, S., Ma ßling, A., Wiedensohler, A., Petäjä, T., Dal Maso, M. and Kulmala, M.: New particle formation in Beijing, China: Statistical analysis of a 1-year data set, J. Geophys. Res., 112(D9), D09209, doi:10.1029/2006JD007406, 2007.

Yao, L., Garmash, O., Bianchi, F., Zheng, J., Yan, C., Kontkanen, J., Junninen, H., Mazon, S. B., Ehn, M.,

https://doi.org/10.5194/acp-2020-1247
Preprint. Discussion started: 24 March 2021

Atmospheric Chemistry and Physics Discussions

638 Paasonen, P., Sipilä, M., Wang, M., Wang, X., Xiao, S., Chen, H., Lu, Y., Zhang, B., Wang, D., Fu, Q., Geng,
639 F., Li, L., Wang, H., Qiao, L., Yang, X., Chen, J., Kerminen, V.-M., Petäjä, T., Worsnop, D. R., Kulmala, M.
640 and Wang, L.: Atmospheric new particle formation from sulfuric acid and amines in a Chinese megacity.,
641 Science, 361(6399), 278–281, doi:10.1126/science.aao4839, 2018.

642 Ye, X., Song, Y., Cai, X. and Zhang, H.: Study on the synoptic flow patterns and boundary layer process of
643 the severe haze events over the North China Plain in January 2013, Atmos. Environ., 124, 129–145,
644 doi:10.1016/J.ATMOSENV.2015.06.011, 2016.

645 Yeo, M.-J., Kim, Y.-S., Yoo, S.-S., Jeon, E.-M. and Kim, Y.-P.: Long-term trend of PM2.5 concentration in
646 Seoul, J. Korean Soc. Atmos. Environ., 35(4), 438–450, 2019.

647 Zhang, R., Wooldridge, P. J., Abbatt, J. P. D. and Molina, M. J.: Physical chemistry of the sulfuric acid/water
648 binary system at low temperatures: stratospheric implications, J. Phys. Chem., 97(28), 7351–7358,
649 doi:10.1021/j100130a038, 1993.

650 Zhang, R., Khalizov, A. F., Pagels, J., Zhang, D., Xue, H. and McMurry, P. H.: Variability in morphology,
651 hygroscopicity, and optical properties of soot aerosols during atmospheric processing, Proc. Natl. Acad. Sci.,
652 105(30), 10291–10296, doi:10.1073/pnas.0804860105, 2008.

653 Zheng, H., Kong, S., Wu, F., Cheng, Y., Niu, Z., Zheng, S., Yang, G., Yao, L., Yan, Q., Wu, J., Zheng, M.,
654 Chen, N., Xu, K., Yan, Y., Liu, D., Zhao, D., Zhao, T., Bai, Y., Li, S. and Qi, S.: Intra-regional transport of
655 black carbon between the south edge of the North China Plain and central China during winter haze episodes,
656 Atmos. Chem. Phys., 19(7), 4499–4516, doi:10.5194/acp-19-4499-2019, 2019.

657

658

659

660

661

662

663

664

https://doi.org/10.5194/acp-2020-1247
Preprint. Discussion started: 24 March 2021

Atmospheric Chemistry and Physics Discussions

665 **Tables**

666 Table 1. Comparison between EOF1 and EOF2 categorized based on size-separated number concentrations
667 measured in Jeju during 2013–2016. (Mean ± 1 standard deviation).

EOF mode	EOF 1	EOF 2
Event Characteristics	Number event	Mass event
	New particle formation (NPF)	No particle burst
Number mode diameter (nm)	< 30	~80–150
Growth Rate$_{10\text{-}50nm}$ (nm h^{-1})	2.1 ± 1.6	-
Condensation Sink$_{10\text{-}25nm}$ (×10^{-2} s^{-1})	0.011 ± 0.020	0.002 ± 0.003
CS$_{100\text{-}470nm}$ (×10^{-2} s^{-1})	1.26 ± 0.86	1.76 ± 1.04
Meteorology	Anticyclone	Synoptic-scale stagnation
Temp. (°C)	13 ± 7	16 ± 8
RH (%)	65 ± 18	73 ± 1.6
Wind direction (mode)	Northeasterly (NE 56%)	Westerly (SW 56%)
Wind speed (m s^{-1})	2.3 ± 1.6	2.7 ± 2.1
Daily solar radiation (MJ m^{-2})	16.5	12.5
Fraction of mid-low cloud (%)	40 ± 30	70 ± 30
Low cloud height (m)	1384 ± 1016	1048 ± 706
Chemical constituents		
OH potential (ppbv*MJ m^{-2})*	63.0 (121.9)	62.8 (115.0)
SO_2 (ppbv)	0.8 ± 0.9	0.7 ± 0.8
NOx	3.9 ± 5.1	4.0 ± 2.7
NH_3	2.5 ± 3.7	2.8 ± 2.4
$PM_{2.5}$ mass (μg m^{-3})	19.1 ± 15.0	26.5 ± 21.3
SO_4^{2-}	2.7 ± 2.8 (14%)	5.4 ± 4.7 (20%)
NO_3^-	1.2 ± 1.9 (6%)	2.6 ± 4.1 (10%)
NH_4^+	1.2 ± 1.5 (6%)	2.7 ± 2.6 (10%)
([SO_4^{2-}]+[NO_3^-])/[NH_4^+]**	1.1	1.0

https://doi.org/10.5194/acp-2020-1247
Preprint. Discussion started: 24 March 2021

Atmospheric Chemistry and Physics Discussions

ALWC (μg m^{-3})***	4.6 ± 7.9	11.6 ± 14.5
Organic carbon (OC)	3.5 ± 22 (18%)	4.1 ± 2.7 (15%)
Elemental carbon (EC)	1.0 ± 0.6 (5%)	1.2 ± 0.7 (5%)

668 * OH potential is the product of daily max solar radiation and max O_3 concentration.

669 ** Equivalent ratio.

670 ***Aerosol Liquid Water Content (ALWC) was calculated using ISORROPIA II with forward mode.

671

672 Table 2. Comparison between two periods ("EOF1 case" and "EOF2 case") occurred during the KORUS-AQ
673 campaign in 2016.

Event	**May 18–20 May**	**May 25–27**
Event characteristics	Persistent anticyclone	Low-level transport and haze development
EOF mode	EOF1: NPF observed	EOF2: $PM_{2.5}$ mass increased
Meteorology		
Temp. (°C) / RH (%)	18 ± 4 / 53 ± 9	18 ± 3 / 73 ± 13
Wind direction* / speed (m s^{-1})	Easterly / 1.6 ± 0.9	Westerly / 1.2 ± 0.6
Boundary layer:		
depth / inversion / stability	deep / weak / unstable	shallow / strong / stable
Free troposphere:		
temp / wind	low /weak northerly	high / strong westerly
Aerosol size–number distribution		
Number mode diameter (nm)	< 60	~100
Volume mode diameter (nm)	198-305	305-470
rBC properties		
rBC mass conc. (μg m^{-3})	0.4 ± 0.1	0.6 ± 0.2
rBC count mode (CMD) (nm)	90	110

https://doi.org/10.5194/acp-2020-1247
Preprint. Discussion started: 24 March 2021

Atmospheric Chemistry and Physics Discussions

rBC mass mode (MMD) (nm)	200	220
rBC coating thickness (nm) * (mean ± 1 SD, 50th, 75th)	29 ± 31, 20, 40	48 ± 39, 40, 75
Chemical constituents		
SO_2 (ppbv)	1.0 ± 0.4	0.7 ± 0.4
NOx (ppbv)	7.0 ± 2.1	4.3 ± 1.6
NH_3 (ppbv)	3.4 ± 8.7	3.8 ± 2.4
$PM_{2.5}$ mass (μg m^{-3})	14.3 ± 5.9	34.5 ± 13.1 (max: 63.0)
SO_4^{2-}	0.7 ± 0.5	6.2 ± 2.7
NO_3^-	0.1 ± 0.2	1.1 ± 1.2
NH_4^+	0.3 ± 0.3	3.3 ± 1.4
([SO_4^{2-}] + [NO_3^-])/[NH_4^+]**	1.0	0.8
ALWC (μg m^{-3})	0.9±0.3	10.3±8.2
Organic carbon (OC)	3.8 ± 1.3	4.1 ± 1.7

* Restricted to 200 ± 20 nm-rBC core; Coating defined as coating thickness ≥ 10 nm considering systematic uncertainty (Laborde et al., 2013).

** Equivalent ratio.

https://doi.org/10.5194/acp-2020-1247
Preprint. Discussion started: 24 March 2021

Atmospheric Chemistry and Physics Discussions

686 **Figures**

687 **Figure captions**

688 **Figure 1. Monthly variation of $PM_{2.5}$ mass concentration at Aewol in Jeju (left) and Bulgwang in Seoul**
689 **(right). The dotted line indicates the national standard of yearly mean $PM_{2.5}$ (15 μg m^{-3}). Shaded**
690 **boxes denote the range of annual mean $PM_{2.5}$ concentrations for 2013-2016.**

691 Figure 2. The two main modes of empirical orthogonal function (EOF) analysis for the number size
692 measurements at Aewol in Jeju from 2013 to 2016. (a) and (b) the diurnal variation of EOF1 and EOF2
693 patterns for each size bin, respectively and (c) and (d) the ambient number size distributions of
694 particles for "EOF1" and "EOF2" days (see Sect. 2 for definition). Note the different color scales for
695 the two cases.

696 Figure 3. Mean diurnal variations of cloud properties and chemical constituents for (a) EOF1 and (b) EOF2.
697 Cloud properties are given for the fraction of mid-low cloud (red) and cloud base height (blue); For
698 reactive gases, SO_2 (red) and NO_2 (blue) concentrations are presented; As major inorganic constituents
699 of $PM_{2.5}$, sulfate (red) and nitrate (blue) are presented with sulfur and nitrogen oxidation ratio, and
700 condensation sink (SOR in red, NOR in green, and CS in blue); and concentrations of OC (red), EC
701 (green), and $PM_{2.5}$ (blue) are shown together in the bottom panel. Points and error bars indicate the
702 hourly mean and standard deviation, respectively.

703 Figure 4. Averaged geopotential height at 925 hPa combined with endpoints of air mass backward trajectories
704 starting at 800 m for (a) EOF1 and (b) EOF2. The color bar is on a logarithmic scale.

705 Figure 5. Aerosol size distributions measured during the 2016 KORUS-AQ campaign at Aewol. (a) Aerosol
706 number size distribution and (b) aerosol volume size distribution. Black boxes indicate two periods:
707 the former for EOF1 case and the letter for EOF2 case. In (b), the black dotted line indicates a peak
708 size where the maximum of volume concentration exists in each sampling duration.

709 Figure 6. Vertical profiles of meteorological parameters and aerosol number concentrations in SMA during the
710 2016 KORUS-AQ campaign. (a) Morning time of May 20, 2019 during "persistent anticyclone"
711 period corresponding to "EOF1 case", (b) morning time of May 25, 2019, and (c) afternoon time of
712 May 25, 2019 during "low-level transport and haze development" period corresponding to "EOF2
713 case". The left panels present ambient temperature (solid blue), relative humidity (dotted red), and
714 deliquescence relative humidity of NH_4NO_3 (sky blue) and $(NH_4)_2SO_4$ (green). The middle panels
715 present wind direction color-coded by wind speed (km h^{-1}). The right panels present number
716 concentrations of particles with Dp > 3.5 nm ($particle_{>3.5\ nm}$) in green, Dp of 0.3–0.5 μm ($particle_{0.3\text{-}0.5}$

https://doi.org/10.5194/acp-2020-1247
Preprint. Discussion started: 24 March 2021

Atmospheric Chemistry and Physics Discussions

717 $_{\mu m}$) in purple, and Dp of 0.5-1.0 μm (particle$_{0.5\text{-}1.0\ \mu m}$) in yellow, and row data in gray open symbol and
718 mean ± standard deviation of each 500 m altitude range in closed symbol with fence. In (c), the vertical
719 profiles of (b) are shown together in light gray. Altitudes of particular interest are shown by shaded
720 gray boxes.

721 Figure 7. The properties of rBC measured during the KORUS-AQ campaign. (a) the relationship between
722 number concentration of particles with > 200 nm in diameter, $PM_{2.5}$ mass concentration, and rBC
723 properties (mass concentration and coating thickness) and (b) the relationship between $PM_{2.5}$ chemical
724 constituents and rBC coating thickness. The measurement data are divided into periods of May 18–20
725 and May 25–27, corresponding to EOF1 and EOF2, respectively.

726

727

728

729

730

731

732

733

734

735

https://doi.org/10.5194/acp-2020-1247
Preprint. Discussion started: 24 March 2021

Atmospheric Chemistry and Physics Discussions

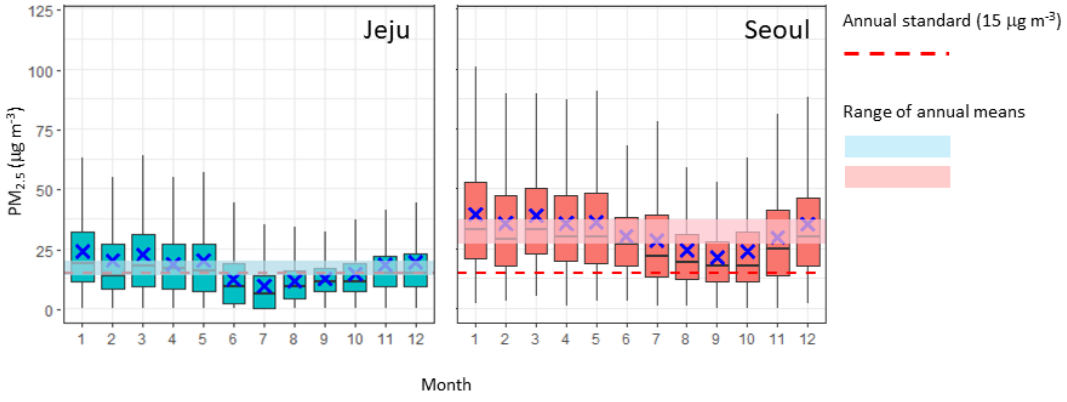

736

737 **Figure 1.**

738

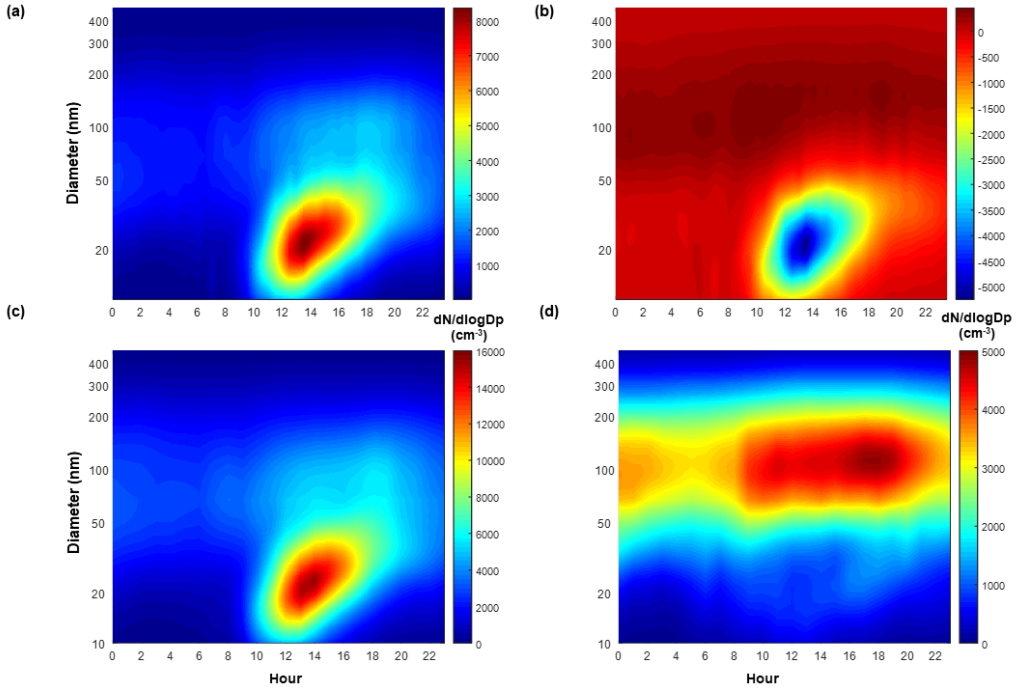

739

740 Figure 2.

741

https://doi.org/10.5194/acp-2020-1247
Preprint. Discussion started: 24 March 2021

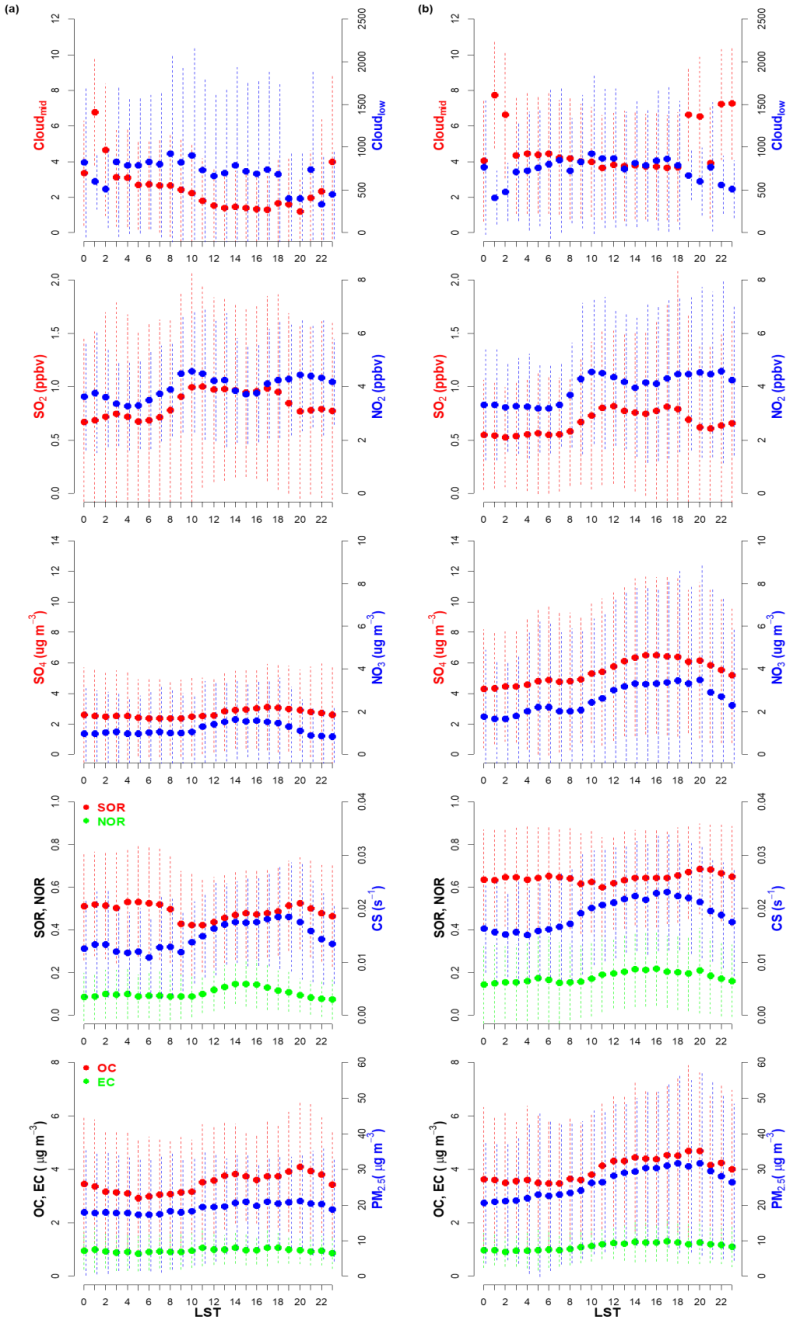

742

743 Figure 3.

https://doi.org/10.5194/acp-2020-1247
Preprint. Discussion started: 24 March 2021

Atmospheric Chemistry and Physics Discussions

744 (a)

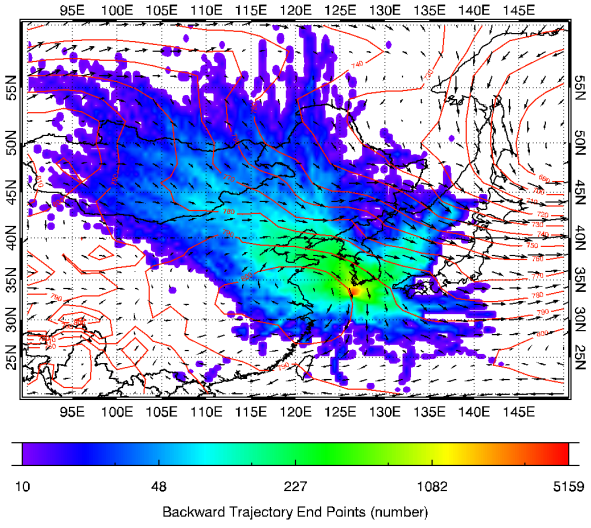

745

746 (b)

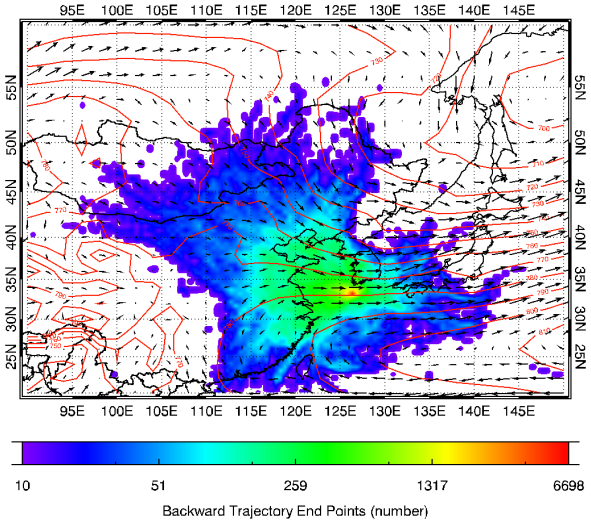

747

748 Figure 4.

749

750

https://doi.org/10.5194/acp-2020-1247
Preprint. Discussion started: 24 March 2021

Atmospheric Chemistry and Physics Discussions

751 (a)

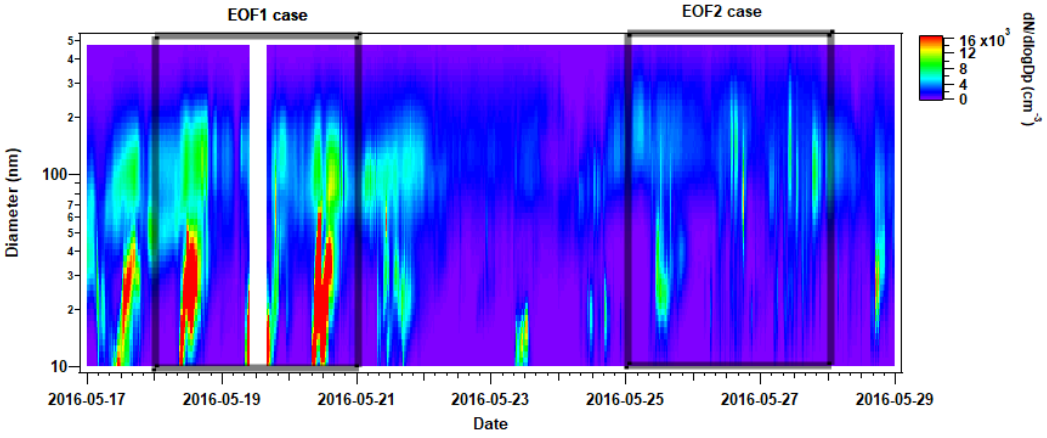

752

753 (b)

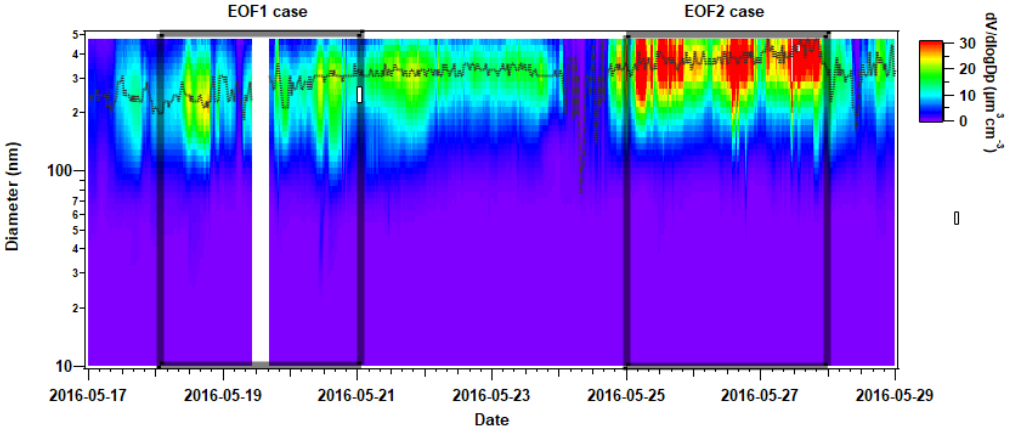

754

755 Figure 5.

756

757

https://doi.org/10.5194/acp-2020-1247
Preprint. Discussion started: 24 March 2021

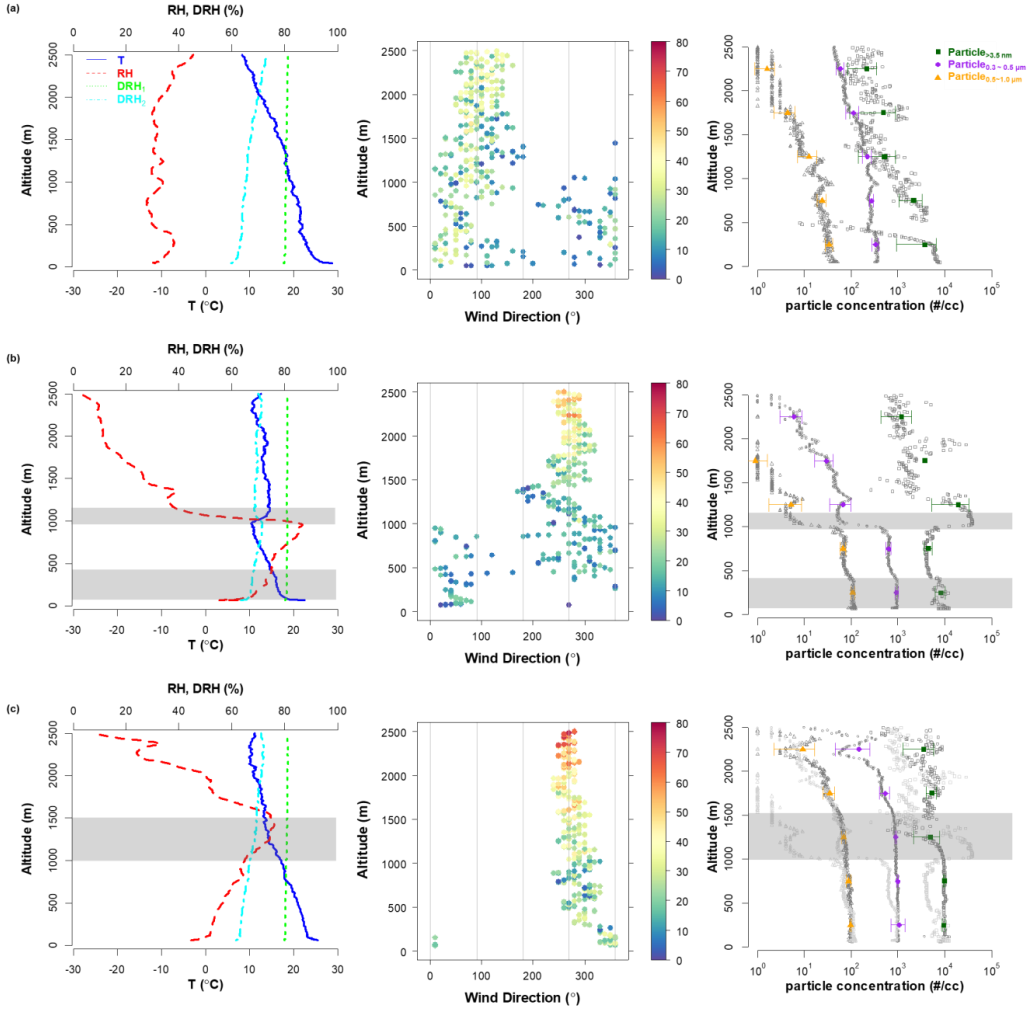

Figure 6.

https://doi.org/10.5194/acp-2020-1247
Preprint. Discussion started: 24 March 2021

Atmospheric Chemistry and Physics Discussions

767 (a)

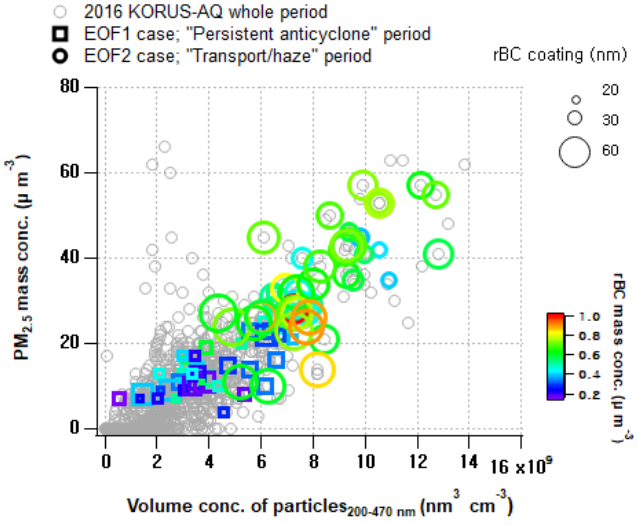

768

769 (b)

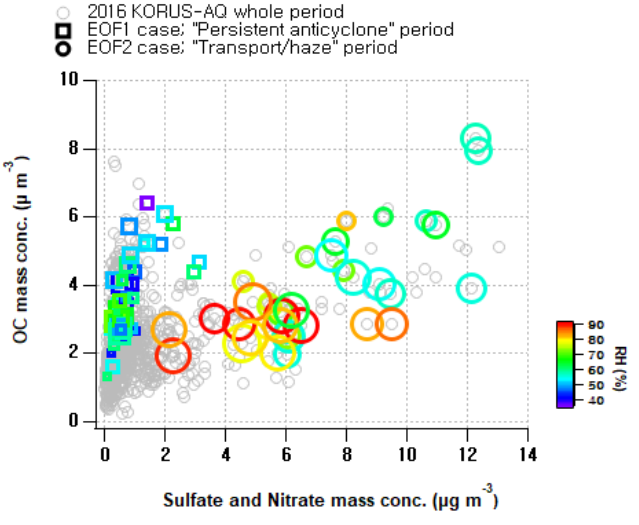

770

771 Figure 7.

772

773